

# MFP-CLIP: Exploring the Efficacy of Multi-Form Prompts for Zero-Shot Industrial Anomaly Detection

Jingyi Yuan, Pengyu Jie, Junyin Zhang, Ziao Li, Chenqiang Gao  
the School of Intelligent Systems Engineering, Sun Yat-Sen University  
{yuanjy36, jiepyu3, zhangjy686, lizao}@mail2.sysu.edu.cn  
gaochq6@mail.sysu.edu.cn

## Abstract

Recently, zero-shot anomaly detection (ZSAD) has emerged as a pivotal paradigm for identifying defects in unseen categories without requiring target samples in training phase. However, existing ZSAD methods struggle with the boundary of small and complex defects due to insufficient representations. Most of them use the single manually designed prompts, failing to work for diverse objects and anomalies. In this paper, we propose MFP-CLIP, a novel prompt-based CLIP framework which explores the efficacy of multi-form prompts for zero-shot industrial anomaly detection. We employ an image to text prompting(I2TP) mechanism to better represent the object in the image. MFP-CLIP enhances perception to multi-scale and complex anomalies by self prompting(SP) and a multi-patch feature aggregation(MPFA) module. To precisely localize defects, we introduce the mask prompting(MP) module to guide model to focus on potential anomaly regions. Extensive experiments are conducted on two widely used industrial anomaly detection benchmarks, MVTecAD and VisA, demonstrating MFP-CLIP’s superiority in ZSAD.

## 1. Introduction

Anomaly detection (AD) holds substantial potential across a wide range of domains, including industrial product quality control, medical diagnostics, etc. Industrial anomaly detection (IAD) focuses on identifying atypical patterns in industrial images. Owing to the scarcity of abnormal samples and the high cost of data annotation, numerous unsupervised anomaly detection methods have emerged [1, 6–8, 11, 21–24, 26, 28–32, 34, 35]. These methods detect and locate defects by measuring deviations from the distribution of normal data. Nevertheless, the vast variability in industrial images, both in terms of object categories and anomaly types, hinders the further development of unsupervised methods.

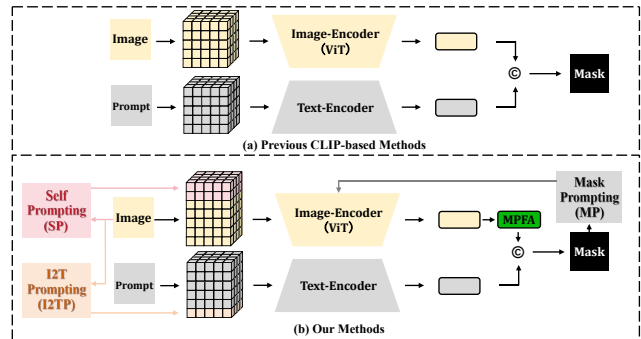


Figure 1. The comparison between previous and our methods based on CLIP. (a) Previous CLIP-based methods obtain mask directly by computing the similarity of patch and text embeddings. (b) Our method introduces image to text prompting (I2TP), self prompting (SP) and multi-patch feature aggregation module (MPFA). With these modules, the model can obtain more detailed object description and focus on potential anomalous regions. A mask prompting (MP) mechanism is also employed to refine the segmentation boundary.

As a result, zero-shot paradigm has been continuously evolving. Its goal is to detect anomalies in novel categories without their participation in the training phase. Recently, many zero-shot anomaly detection (ZSAD) methods [3–5, 10, 37–39] rely on pre-trained vision language models (VLMs) for utilizing their strong generalization capability. Owing to the CLIP [19]’s remarkable transferability to downstream tasks, great image-text alignment and representation capability, many CLIP-based ZSAD methods [3, 5, 20, 38, 39] have emerged. These methods compute the similarity of visual and text embeddings from CLIP as anomaly map, as presented in Figure 1(a). The text embeddings are extracted just by the text template.

WinCLIP [10] employed pre-trained VLMs with manually designed prompts without any additional fine-tuning or training. However, the pre-trained CLIP is trained on natural image datasets deviating from industrial image datasets,

resulting WinCLIP’s certain limitations in IAD. To overcome the limitations, some methods [3, 38, 39] used auxiliary industrial data for fine-tuning. In particular, AnomalyCLIP [39] used additional data to transfer models from the natural image domain to the industrial image domain. AdaCLIP [3] introduced a hybrid semantic fusion module to capture semantic-rich image feature, enhancing the performance of anomaly detection. Despite these efforts, accurately localizing small and logistic defects remains challenging. They manually design text prompts to describe object and their state (normal/ abnormal), struggling to generalize all images, leading suboptimal performance. Additionally, there are few methods involving visual prompts to refine the patch embeddings and emphasize on the specific regions.

To address the aforementioned problems, we propose a new framework, named MFP-CLIP, which is built on CLIP. As shown in Figure 1(b), our method employs an image-text prompting (I2TP) module to supply the detailed object description except the text prompt template. To enhance the image representations and perception of potential anomaly regions. The self-prompting (SP) and mask-prompting(MP) mechanisms are introduced. SP uses image features from CNN as visual prompts for itself to acquire a more detailed local embeddings for specific image. And then, we integrate the prompts with patch embeddings from vision transformer (ViT) to obtain deep representations, combining local and global context perception. The MP mechanism is served as a boundary refiner that leverages segmented masks as visual prompts, guiding the model to focus more precisely on potential anomalous regions. Moreover, to strengthen the capability of detecting small and complex defects, we introduce a multi-patch feature aggregation (MPFA) module that refines feature representations through the neighborhood patch embeddings to enhance spatial continuity and contextual consistency. Both SP and MPFA enable model suitable for multi-scale anomalies, especially for small and complex anomalies.

The main contributions are summarized as follows:

- We propose MFP-CLIP, a novel framework built upon CLIP to enhance the detection of unseen objects. Visual and textual embeddings are combined to obtain more detailed object description with I2TP. We employ self prompting (SP) and mask prompting (MP) to adapt the patch embeddings and focus on the potential anomalous regions.
- A multi-patch feature aggregation (MPFA) strategy is introduced to enhance the feature perception between neighborhood patches.
- Extensive experiments are conducted on two main industrial datasets, MVTeHcAD [2] and VisA [41]. MFP-CLIP presents its superiority in zero-shot anomaly detection.

## 2. Related Work

### 2.1. Anomaly Detection

Given that abnormal data in industrial domain is scarce and costly, it is hard to collect plenty of defective images for training. Thus, there are two main paradigms which mostly follow the one-model-one-class manner.

**Unsupervised Anomaly Detection** methods rely exclusively on normal samples within target categories, which model the distribution of normal images when training, and acquire the deviation between test samples with normal distribution to locate anomalies. Embedding-based methods [1, 6–8, 13, 21–27, 32, 35] commonly use pre-trained models to extract features of normal samples and then model the distribution of the normal feature. These methods realize remarkable performance on target categories but face serious performance degradation when testing unseen objects. Methods based on memory-bank like Patch-Core [6, 7, 22] need extra space to store normal feature, limiting the inference speed. Reconstruction-based approaches [11, 14, 28–31, 33, 34, 36] make an assumption that the model trained only on normal samples is unable to accurately reconstruct abnormal samples. But these methods usually have a strong generalization capability to defective regions, resulting the reconstruction result almost equals the input image.

**Semi-Supervised Anomaly Detection** methods [9] utilize normal samples and several abnormal images to implement better performance comparing to unsupervised anomaly detection methods. Although they acquire performance enhancing by exploiting defective images, they struggle to unseen categories as unsupervised AD does.

### 2.2. Prompt Learning

As an emerging technology in the field of natural language processing, prompt learning has received extensive attention in recent years. The core idea is to design appropriate prompts to guide the pre-trained model to adapt to a specific task, without the need for a large amount of task-specific annotated data. With the deepening of research, prompt learning has gradually expanded from a single text task to a multi-modal domain. For instance, CoOp [37] employs learnable prompt tokens into text branch, first introducing prompt learning in CLIP. Subsequently, DenseCLIP [20] and CoCoOp [38] use visual context prompting to adapt VLMs to the target domain. In this work, we propose self prompting mechanism to take global and local context comprehension into account simultaneously, better detecting small and complex anomalies.

### 2.3. Zero-Shot Anomaly Detection

Recently, large visual-language pre-trained models such as MiniGPT-4 [16], LLaVA [12], Otter [40] and CLIP [19] present promising zero-shot abilities. Especially, CLIP

draws much attention, which aims to align the feature space of vision and language modalities. Zero-Shot Anomaly Detection methods [3–5, 10, 20, 37–39] often utilizes a few auxiliary seen objects and anomalies during training to identify novel categories, relying on remarkable generalization capability of VLMs. Given the strong image-text alignment and generalization ability fo the pre-trained VLM named CLIP [19], many off-the-shelf ZSAD methods select CLIP as baseline. In particular, WinCLIP [10] designs normal/abnormal text prompts manually, and then computes the cosine similarity between image feature embedding and text feature embedding, subsequently followed by an interpolation module to obtain anomaly map. In contrast to the training-free method, some [4, 5, 39] employ annotated auxiliary data to train one linear adapter, reducing the gap between natural and industrial domains. However, considering the expensive cost and low efficiency of hand-crafted prompts, AnomalyCLIP [39] introduces two unified learnable text prompts for normal/abnormal states to reduce labors and time consumption, resulting in a better ZSAD performance. In this work, we explore the efficacy of multi-form prompts to exploit CLIP for ZSAD.

### 3. Method

#### 3.1. Problem Definition

Given one certain test sample  $I \in \mathbb{R}^{H \times W}$ , zero-shot anomaly detection methods aim to produce image-level anomaly score  $S \in [0, 1]$  and pixel-level anomaly map  $M \in [0, 1]^{H \times W}$ . Following the generalized ZSAD methods mentioned in Section 2.3, we leverage an auxiliary dataset  $D_a = \{(I_1, G_1), \dots, (I_n, G_n) \mid G_i \in [0, 1]^{H \times W}\}$  for training, which consists of both normal and abnormal samples with corresponding annotations. And we test in unseen dataset  $D_t = \{I_{t_1}, \dots, I_{t_n}\}$ . Notably, the auxiliary dataset and test dataset originate from different domains, ensuring that  $D_a \cap D_t = \emptyset$ .

#### 3.2. Overview

We adopt CLIP as the backbone of our framework, MFP-CLIP. An overview of our method is illustrated in Figure 2. CLIP is used to extract both image and text features, mapping them into a shared embedding space. To fully leverage CLIP’s image-text alignment capability, we detect and localize anomalies by computing the cosine similarity between visual and textual embeddings, following the approach of previous works [5, 10].

In the image branch, one image is input into CLIP image encoder, obtaining the patch embeddings. The self prompting (SP) module generates the CNN-based local feature for itself, refining the patch embeddings. The refined feature will be followed by a linear projection and a multi-patch feature aggregation (MPFA), adapting the feature dimen-

sion and aggregating multi-scale features, respectively. In the text branch, we employ the image to text Prompting (I2TP) mechanism to enhance textual prompts by integrating visual features, allowing for better representations of the object. Then, we compute the cosine similarity between the aggregated patch embeddings with more detailed textual embeddings as the coarse anomaly map. Finally, the coarse segmentation results serve as mask-form prompts to emphasize on the potential anomalous regions, refining the boundaries. By integrating these modules, MFP-CLIP effectively enhances CLIP’s ability to detect and localize anomalies in unseen categories with improved precision and robustness.

#### 3.3. Image to Text Prompting (I2TP)

Our method introduces Image to Text Prompting module across visual and textual modalities to enhance anomaly detection. In the text branch, previous approaches rely solely on manually designed prompts, which struggle to capture fine-grained details of object categories. To address this limitation, we use the I2TP, integrating image features from CNN into text tokens. As illustrated in Figure 2, a test image  $I_{t_i} \in \mathbb{R}^{H \times W}$  is fed into ResNet-50, and the extracted feature embedding is flattened, yielding  $F_{cnn} \in \mathbb{R}^{1 \times D_v}$ . Given the inherent differences between visual and textual features, we add one multilayer perceptron (MLP) as described in Eq (1), simultaneously aligning their dimension.

$$\tilde{F}_{cnn} = Linear(F_{cnn}), \tilde{F}_{cnn} \in \mathbb{R}^{1 \times D_t}, \quad (1)$$

Subsequently, we concatenate the text tokens  $P_t \in \mathbb{R}^{n \times D_t}$ , generated from "A photo of a normal/abnormal [OBJ]", with the transformed image feature  $\tilde{F}_{cnn}$ , forming enhanced textual prompt tokens  $\tilde{p}_t$ . Moreover, to ensure token consistency, we introduce an additional linear projection before feeding the tokens into the text encoder. The process follows,

$$\tilde{P}_t = concat(p_t, \tilde{F}_{cnn}), \quad (2a)$$

$$\hat{P}_t = Linear(\tilde{P}_t), \quad (2b)$$

$$F_t = Encoder_t(\hat{P}_t), \quad (2c)$$

where,  $concat(\cdot, \cdot)$  and  $Linear(\cdot)$  denote concatenation and linear projection along the second dimension, respectively. The final text feature embeddings are represented as  $F_t$ .

#### 3.4. Self Prompting (SP)

Inspired by text prompt, we hypothesize that visual prompts will be beneficial to visual representation and comprehension for special image. We employ a self-prompting mechanism, where the model uses image features to generate visual prompts for itself. Since ViT is selected as the image encoder, we leverage CNN-extracted features as visual

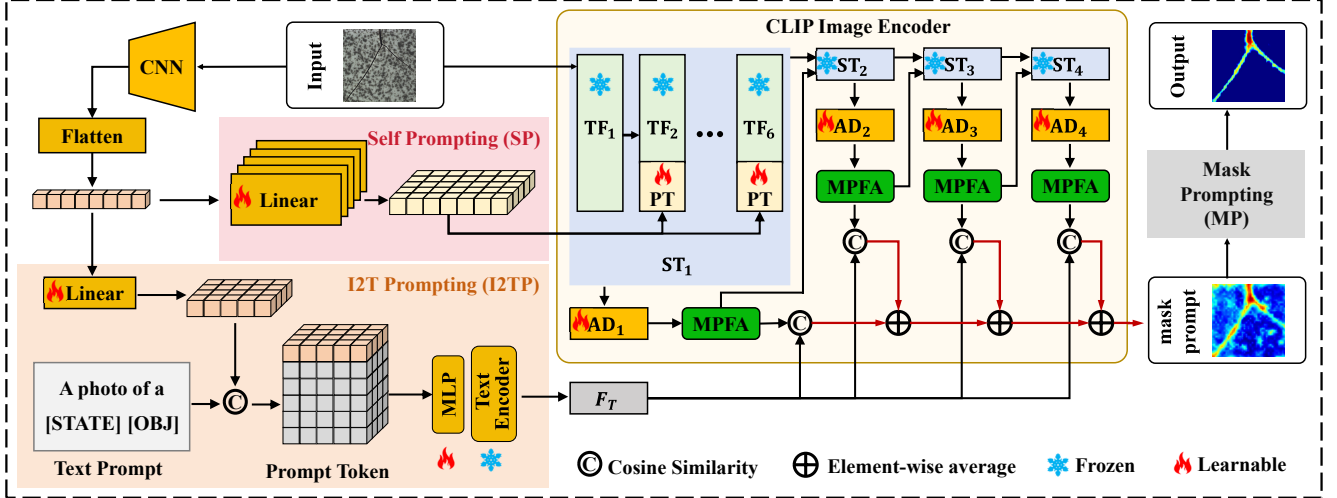


Figure 2. Framework of MFP-CLIP. Our methods consist of four modules. Self Prompting (SP): uses image features to generate visual prompts for itself, refining the patch embeddings from ViT. I2T Prompting (I2TP): integrates image features from CNN into text tokens to capture fine-grained details of object categories. Multi-Patch Feature Aggregation (MPFA): conducts adaptive average pooling over  $N \times N$  neighborhood patches to enhance multi-scale embeddings. Mask Prompting (MP): employs coarse anomaly map as a mask-form visual prompt to emphasize on the potential anomaly regions.

prompts to benefit from both ViT’s global reasoning and CNN’s local feature extraction. In detail, we employ  $K$  linear projection adapters to transform the CNN features into visual prompts  $P_v$ , aligning the feature dimensions across different architectures. The feed-forward process is,

$$P_v = [Linear_i(F_{cnn})]_{i=1}^K, P_v \in \mathbb{R}^{K \times D_v}, \quad (3)$$

where  $[\cdot]$  denotes concatenation along 1st dimension.

As mentioned in Section 3.3, we acquire the visual prompt  $P_v$  by encoding image with CNN. While this visual prompt is designed for individual images during both training and testing, a unified visual prompt—similar to text template—is essential for better generalization. To achieve this, we create  $K$  learnable prompt tokens  $PT \in \mathbb{R}^{K \times D_v}$  and combine  $PT$  with  $P_v$  to form the final visual prompt tokens, as formulated in Eq (4). Here  $concat(\cdot, \cdot)$  denotes concatenation along the token dimension.

$$P_v = concat(P_v, PT), \quad (4)$$

Unlike the text branch, the visual branch requires aggregation between feature tokens extracted from two different frameworks (CNN and ViT). In ViT, self-attention effectively captures global context, allowing any token in the input sequence to influence the output. To leverage this property, we integrate the local and global features from multi-framework by the self-attention mechanism. In particular, there are 24 transformers in the CLIP image encoder, where we divide all the layers into 4 stages, as illustrated in Figure 2. To effectively integrate local context while preserving

global modeling capability, we perform alignment operations only in the first stage  $ST_1$ .

More precisely, the first stage comprises six layers. To retain all contextual information from the original image, we leave the first layer unchanged. In the 2nd to 6th layers, we first remove the last  $K$  tokens from the original Transformer layer’s output  $F_v \in \mathbb{R}^{P_n \times D_v}$ . And then, the remaining feature tokens of transformer layer and the modified visual prompt tokens are concatenated. This process is formulated as follows,

$$F_{v_1} = TF_1(I), \quad (5)$$

$$F_{v_i} = TF_i(concat(F_{v_{i-1}}[: -K], P_v)), i = 2, \dots, 6, \quad (6)$$

where,  $TF_i(\cdot)$  and  $concat(\cdot, \cdot)$  denotes self-attention mechanism and concatenation along the first dimension, respectively. It’s noting that SP not only integrates CNN’ strong local feature extraction with ViT’s powerful global context modeling, but also transfers the CLIP image encoder from the natural image domain to specialized domains through training on auxiliary data. This cross-framework alignment ensures robust feature representation and enhances the model’s ability to detect domain-specific anomalies.

### 3.5. Multi-Patch Feature Aggregation (MPFA)

To compute the cosine similarity between image and text embedding, their feature dimensions must be identical. However, considering the inherent dimensional discrepancy in the original CLIP model, we use a set of linear adapters  $\{AD_i | i \in \{1, 2, 3, 4\}\}$  to ensure dimensional alignment, as APRIL-GAN [4] does. Additionally, as CLIP is pre-trained

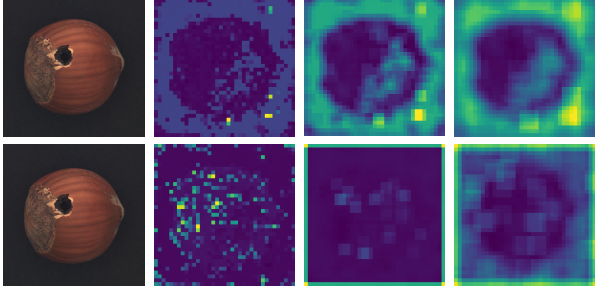


Figure 3. Visualization of aggregated feature. The first column is original image, the second column presents the raw patch embeddings, and the second and third columns illustrate the embeddings aggregated over  $3 \times 3$  and  $5 \times 5$  neighborhood patches, respectively. The first and second rows correspond to  $\tilde{F}_{v_i}^N[:, 0]$  and the averaged patch embeddings along the last dimension of  $\tilde{F}_{v_i}^N$ , respectively.

on natural images, there exists a domain gap when applying it to our downstream task. So the adapters can also contribute to transferring CLIP from natural domain to industrial domain. Each adapter consists of two linear projection layers and two activation layers, processing the patch embeddings at different stages. Here,  $AD_i(\cdot)$  denotes the  $i$ -th linear projection layer.

$$F_{v_i} = AD_i(F_{v_i}), \quad (7)$$

ViT divides an image into multiple patches and encodes them using self-attention mechanism. To ensure smoother representations at patch boundaries and integrate the context between surrounding patches, we design a Multi-Patch Feature Aggregation (MPFA) module. MPFA enhances local context awareness by applying adaptive average pooling (AAP) over neighborhood patches. In order to make the contour of object and defect more vivid, we aggregate features within an  $N \times N$  neighborhood for each patch, where  $N$  controls the scale of feature aggregation and is set to 3 by default.

In particular, at the  $i$ -th stage  $ST_i$ , we obtain the adapted patch embedding  $F_{v_i} \in \mathbb{R}^{P_n \times D_v}$ , as formulated in Eq (7), where  $P_n$  denotes the numbers of patches. For each patch, the embedding is stored as a feature vector. To facilitate AAP, we first reshape  $F_{v_i}$  into a grid representation  $\tilde{F}_{v_i} \in \mathbb{R}^{\sqrt{P_n} \times \sqrt{P_n} \times D_v}$ . We then apply adaptive average pooling over each patch's  $N \times N$  neighborhood, followed by reshaping the aggregated embeddings back to the original format,

$$\tilde{F}_{v_i} = \text{reshape}(F_{v_i}), \quad (8)$$

$$\tilde{F}_{v_i}^N = \text{AAP}(\tilde{F}_{v_i}), \quad (9)$$

$$\tilde{F}_{v_i}^N = \text{reshape}(\tilde{F}_{v_i}^N), \quad (10)$$

As shown in Figure 3, we compare the attention map of patch embeddings before and after adaptive average pooling over  $N \times N$  neighborhood patches. The results demonstrate that after MPFA, patch boundaries in the feature map become more distinct and prominent, allowing the model to focus on larger, more complex anomalies. This enhancement significantly improves the model's capability to detect complex objects and defects.

### 3.6. Mask Prompting (MP)

After aggregating the multi-patch features, we obtain the refined patch embeddings  $\tilde{F}_{v_i}^N$ . Following existing methods, we compute the similarity of image and text features to obtain the results,

$$M_{I_i} = \text{Interpolate}(\text{Softmax}(\cos(\tilde{F}_{v_i}^N, F_t))), \quad (11)$$

$$M_I = \text{mean}\left(\sum_{i=1}^4 M_{I_i}\right), \quad (12)$$

$$S = \text{max}(M_I), \quad (13)$$

here,  $\cos(\cdot, \cdot)$  and  $\text{mean}(\cdot)$  denotes cosine similarity and average operation.  $\text{max}(\cdot)$  represents the maximum along the last two dimensions. The function *Interpolate* refers to bilinear interpolation.

Although these modules discussed in Section 3.3 to Section 4.3 significantly enhance model performance, a common issue persists: the segmentation results often exhibit imprecise contours, especially for complex and small anomalies. Additionally, the detected anomaly regions tend to be slightly larger than the ground truth. To tackle this drawback, we design one mask prompting module to refine the boundary.

After processing an image  $I$  through the MFP-CLIP model, we can get the pixel-level anomaly map  $M \in [0, 1]^{H \times W}$  and the image-level anomaly score  $S \in [0, 1]$ . Here, the value of each pixel,  $M(i, j)$ ,  $i, j \in \mathbb{N}$ , represents the anomaly probability at location  $(i, j)$ —the higher the value is, the more likely the region contains a defect. Therefore, we leverage this coarse anomaly map as a mask-form visual prompt to guide the model in focusing more precisely on critical regions.

Specifically, as illustrated in Figure 4, to emphasize those potential anomaly regions, we apply element-wise multiplication between the coarse anomaly map  $M$  and the input image  $I$ , outputting a modified image  $\tilde{I}$ . Since original image and modified image belong to the same modality, we employ the modified image embeddings as mask prompts directly, concatenating them with the original image embeddings in the transformer layer. The feed-forward process is,

$$\tilde{I} = I \odot M, \quad (14)$$

$$F_I = PatchEmbedding(I) + E_{pos}(I), \quad (15)$$

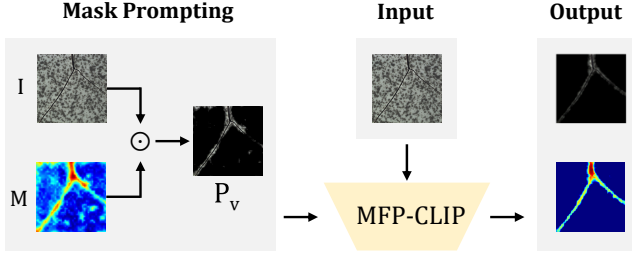


Figure 4. Framework of mask prompting (MP)

$$F_{\tilde{I}} = PatchEmbedding(\tilde{I}) + E_{pos}(\tilde{I}), \quad (16)$$

$$F_I = Linear(concat(F_I, F_{\tilde{I}})), \quad (17)$$

$$F_v = Encoder(F_I), \quad (18)$$

where  $\odot$  denotes element-wise multiplication.  $E_{pos}(\cdot)$  represents positional embeddings,  $PatchEmbedding(\cdot)$  divides image into patches and  $Encoder(\cdot)$  is the image encoder. The remaining steps follow the same procedure as the MFP-CLIP model.

To optimize the anomaly map  $M$ , we employ focal loss [15] and dice loss [18], which effectively handle class imbalances and enhance segmentation accuracy. Meanwhile, for the anomaly score  $S$ , we utilize binary cross-entropy (BCE) loss [17] for training.

## 4. Experiments

### 4.1. Experimental Setup

**Datasets.** To validate our model MFP-CLIP, we conduct experiments on two widely used industrial anomaly detection datasets, MVTechAD [2] and VisA [41]. MVTech AD is a dataset for benchmarking anomaly detection methods with a focus on industrial inspection. It contains over 5000 images with a high-resolution of  $700 \times 700$  to  $1024 \times 1024$ . They are divided into fifteen different objects (10) and textures (5) categories. Each category comprises a set of defect-free training images and a test set of images with various kinds of defects as well as images without defects. The VisA dataset contains 12 subsets corresponding to 12 different objects, containing 10,821 images with 9,621 normal and 1,200 anomalous samples. The image in it has a high-resolution of  $1000 \times 1000$  to  $1500 \times 1500$ . Both of MVTechAD and VisA contain original image and pixel-level annotations.

**Evaluation Metrics.** Following most ZSAD methods, we select image-level and pixel-level Area Under the Receiver Operating Characteristic Curve (I-AUC, P-AUC) to compare the performance with other ZASD approaches in anomaly detection and localization.

**Implementation Details.** Our experiments select the pre-trained CLIP with ViT-L-14@336 by OpenAI as default backbone. The image size is resized to  $518 \times 518$  both for training and testing. In particular, we divide the image encoder into 4 stages from 24 transformer layers, extracting image patch embeddings from 6th, 12th, 18th, 24th layers. Due to the unseen objects in test, we select one from MVTechAD, VisA as auxiliary dataset for training and the other as testing dataset. The number  $K$  of adapters for CNN features is set to five which means the size of visual prompt is  $5 \times D$ . The aggregation scale  $N$  is also set to five as default. The model is trained for 100 epochs with the batch size of 1. we use Adam optimizer with an initial learning rate (lr) of 0.001, and the lr decay factor is  $1/(epoch + 1)$ . All experiments are conducted with a single NVIDIA GeForce RTX 3090 24GB GPU.

**Comparison Methods.** To better evaluate our model, we compare our proposed MFP-CLIP with two kinds of methods: training-free and training with auxiliary data methods. For the training-free methods, we select WinCLIP [10] for comparison, the first and representative CLIP-based method and requesting no auxiliary data for training. For the second kind of methods, we select APRIL-GAN [4], AdaCLIP [3] and AnomalyCLIP [39] for comparison, training on auxiliary data and testing on unseen objects as we do.

### 4.2. Comparisons with the-state-of-art methods

**Quantitative results** on MVTechAD and VisA are reported in Table 1. Bold and underlined values denote the best and the second best results, respectively. It can be observed that our proposed MFP-CLIP outperforms all compared methods on metric AUC. AnomalyCLIP employing learnable text prompts and AdaCLIP using hybrid semantic fusion present the suboptimal performance. On MVTechAD, our method exceeds AnomalyCLIP and AdaCLIP by 0.7% and 3.0% I-AUC, respectively. And for anomaly localization, MFP-CLIP achieves 92.1% P-AUC, 1.0% higher than the second best method. We also conduct experiments on the challenging VisA dataset. As shown in Table 1, our MFP-CLIP achieves the best performance in both anomaly detection and localization with 87.9% I-AUC and 96.0% P-AUC, outperforming the second best result by 1.0% I-AUC and 0.5% P-AUC, respectively. The quantitative comparison demonstrates our superiority over other ZSAD methods. The detailed quantitative results of all categories on MVTechAD and VisA will be reported in the Supplementary Material.

**Qualitative result** on MVTechAD and VisA are shown in Figure 5(a) and Figure 5(b), respectively. There are many small defects like broken teeth in zipper and complex defects like broken-large in bottle. The boundary of their ground truth is quite fine-grained. Figure 5(a) presents the

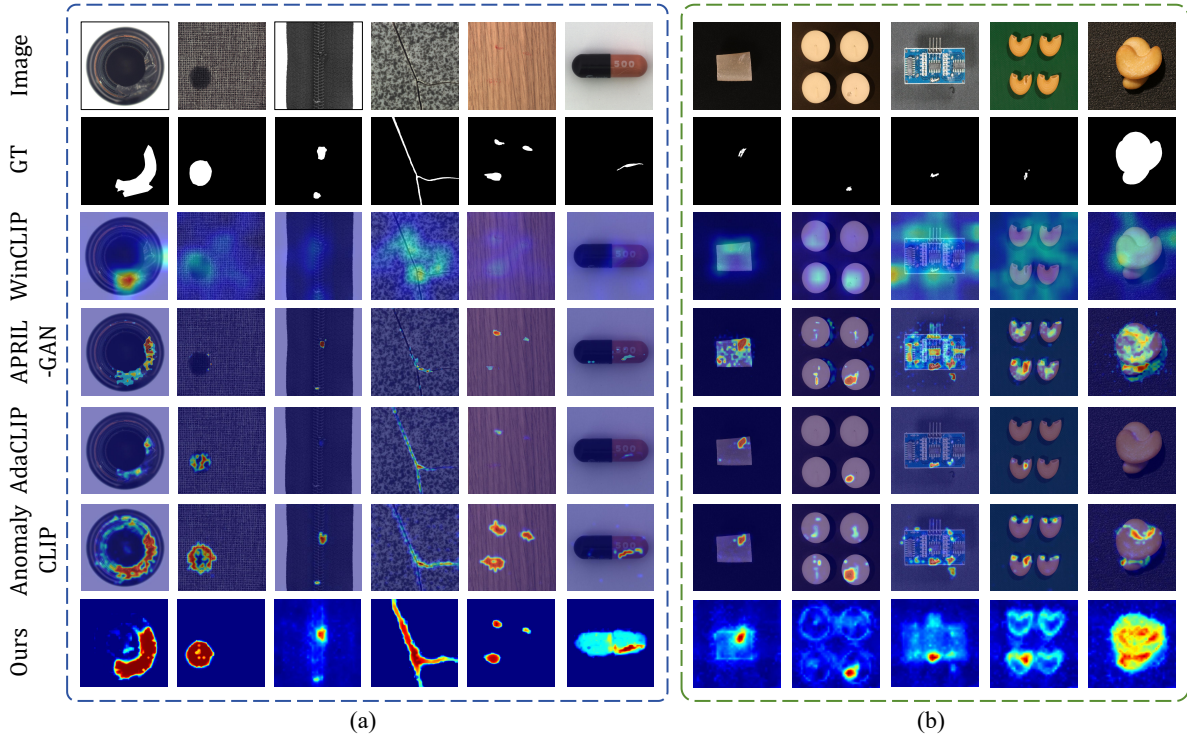


Figure 5. Visualization of ZSAD methods. (a) and (b) present the localization results on MVTechAD and VisA, respectively.

Table 1. Detection and localization results of ZSAD methods on MVTechAD and VisA. **Bold** and underlined indicate the best and the second best results, respectively.

Task	Dataset	WinCLIP [10]	APRIL-GAN [4]	AnomalyCLIP [39]	AdaCLIP [3]	<b>Ours</b>
Detection (I-AUC)	MVTec AD	91.8	82.3	<u>91.5</u>	89.2	<b>92.2</b>
	VisA	78.1	81.7	82.1	<u>85.8</u>	<b>87.9</b>
Localization (P-AUC)	MVTec AD	85.1	83.7	<u>91.1</u>	88.7	<b>92.1</b>
	VisA	79.6	95.2	95.5	<u>95.5</u>	<b>96.0</b>

qualitative results of these methods on MVTechAD, where our method can localize the contour of small and complex anomalies more accurately. In contrast, the pixel-level results of categories like tile, carpet and wood demonstrate MFP-CLIP’s superiority in detecting and localizing defects. We attribute the remarkable performance to the refined features by SP, MPFA and MP module. Moreover, the visualization results on VisA are shown in Figure 5(b). Our masks are more closed to the ground truth while other methods tend to segment the rough boundary larger than the ground truth. In contrast, our proposed MFP-CLIP can outline the contour of defects more exactly and our false-positive regions are less than others, which demonstrate the great efficacy multi-form prompts for zero-shot industrial anomaly detection.

### 4.3. Ablation Study

We conduct ablation studies on MVTechAD to assess the influence of all components in MFP-CLIP. Table 2 reports the importance of every individual component, demonstrating the contribution of each module to the overall performance. Single-component ablation can clearly identify the importance of each component and improve the understanding of how the model works. Moreover, we also conduct an degree analysis by varying the number of patch embeddings aggregated during the multi-patch feature aggregation (MPFA) process, as well as the number of stages where self prompting (SP) module is employed. The performance comparison of varying hyper-parameters is present in Table 3 and Table 4, respectively.

**Ablation for image to text prompting (I2TP) module.** As reported in Table 2, the performance gain from the fourth

Table 2. The influence of different components in MFP-CLIP.

I2TP	SP	MPFA	MP	I-AUC	P-AUC
✓	✓	✓	✗	91.1	90.8
✓	✓	✗	✓	91.5	91.1
✓	✗	✓	✓	90.2	90.0
✗	✓	✓	✓	90.3	90.3
✓	✓	✓	✓	92.2	92.1

row to last row demonstrates superiority of I2TP module. The manually designed text prompts like “a photo of a normal/abnormal [object]” struggle to represent the detailed object (category) and state (normal/abnormal) information. Without I2TP module, the text embeddings are only extracted from the text template. The performance decreases by 1.9% I-AUC and 1.8% P-AUC. This is because the I2TP prompts extracted from CNN introduce the local context into text prompts. They provide more detailed region information, helping model better understand object category and the spatial distribution of features. The text branch is able to produce more fine-grained and precise textual embeddings that guide the model in identifying anomalies with greater accuracy.

**Ablation for self prompting (SP) module.** To assess the impact of the SP module, we conduct an ablation experiment comparing the performance of MFP-CLIP with and without SP on the MVTechAD dataset. As shown in the third row in Table 2, without SP, the model extract image feature by ViT, showing a suboptimal performance. Without the alignment of CNN features, the model struggles to capture detailed local context. In contrast, enabling the SP module allows the model to effectively align features from both CNN and ViT, enabling the fusion of local and global representations. For instance, the I-AUC and P-AUC increases by 2.0% and 2.1%, respectively. Moreover, we present the performance when employing SP on different stages in Table 4. Notably, when it is employed into 2nd to 4th stages, the performance doesn’t show a significant improvement. This may contribute to the self-attention mechanism, which has established the interaction between cross-framework features. To reduce computation cost, we employ SP only on the first stage.

**Ablation for multi-patch feature aggregation (MPFA).** To assess the importance of Adaptive average pooling over  $N \times N$  neighborhood patch embeddings, where  $N$  is set to 3 in default. we conduct corresponding ablation study as shown in Table 2. When it comes to small and complex defects like crack in pill and bent wire in cable, the MPFA module can enhance the performance of localizing their boundary, which results in an increase of 0.7% in I-AUC and 1.0% in P-AUC. Additionally, we search for the best value of  $N$  by comparing the results of

Table 3. The different values of  $N$  in MPFA.

Scale	I-AUC	P-AUC
$1 \times 1$	91.5	91.1
$3 \times 3$	92.2	92.1
$5 \times 5$	91.8	91.7

Table 4. The employment of SP on different stages.

Stage	I-AUC	P-AUC
$ST_1$	92.23	92.11
$ST_{1-2}$	92.27	92.14
$ST_{1-3}$	92.19	92.04
$ST_{1-4}$	91.96	91.87

{1, 3, 5} reported in Table 3. The visualization of patch embeddings aggregated by different sizes is illustrated in Figure 3. Properly aggregating the neighborhood patch embeddings can contributes to the bigger scale and complex defects, while the feature will be vague if  $N$  is too big.

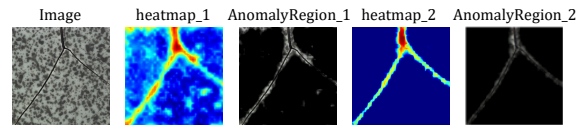


Figure 6. Visualization of the segmentation masks before and after MP module.

**Ablation for mask prompting (MP) module.** As presented in Figure 6, without the MP module, the segmentation results remain imprecise with contours still lacking sharpness and anomaly regions being slightly larger than the ground truth. When incorporating the MP as visual prompts, the model demonstrates improved localization from 90.8% to 92.1% P-AUC. The anomaly region becomes more vivid and the false-positive regions decreases.

## 5. Conclusion

In this paper, we propose MFP-CLIP, a generalized method through cross-framework feature alignment and boundary refinement to optimize anomaly localization, especially for small and complex defects. By using image to text prompting (I2TP) to enhance text prompts, MFP-CLIP better represents the object in the image, allowing for more accurate anomaly detection. The self prompting (SP) module combines global and local features. And multi-patch feature aggregation (MPFA) is also introduced to enhance the perception of complex and small anomalies. Finally, through mask prompting(MP), the contours of anomalies are modified from coarse to fine-grained. Extensive experiments are conducted on two main industrial datasets, demonstrating MFP-CLIP’s superiority in zero-shot anomaly detection.



## References

- [1] Kilian Batzner, Lars Heckler, and Rebecca König. Efficientad: Accurate visual anomaly detection at millisecond-level latencies. In *Proceedings of the IEEE/CVF Winter Conference on Applications of Computer Vision (WACV)*, pages 128–138, 2024. 1, 2
- [2] Paul Bergmann, Michael Fauser, David Sattlegger, and Carsten Steger. Mvtec ad — a comprehensive real-world dataset for unsupervised anomaly detection. *2019 IEEE/CVF Conference on Computer Vision and Pattern Recognition (CVPR)*, pages 9584–9592, 2019. 2, 6
- [3] Yunkang Cao, Jiangning Zhang, Luca Frittoli, Yuqi Cheng, Weiming Shen, and Giacomo Boracchi. Adaclip: Adapting clip with hybrid learnable prompts for zero-shot anomaly detection. *ArXiv*, abs/2407.15795, 2024. 1, 2, 3, 6, 7
- [4] Xuhai Chen, Yue Han, and Jiangning Zhang. A zero-/few-shot anomaly classification and segmentation method for cvpr 2023 vand workshop challenge tracks 1&2: 1st place on zero-shot ad and 4th place on few-shot ad. *ArXiv*, abs/2305.17382, 2023. 3, 4, 6, 7
- [5] Xuhai Chen, Jiangning Zhang, Guanzhong Tian, Haoyang He, Wuhao Zhang, Yabiao Wang, Chengjie Wang, Yunsheng Wu, and Yong Liu. Clip-ad: A language-guided staged dual-path model for zero-shot anomaly detection. *ArXiv*, abs/2311.00453, 2023. 1, 3
- [6] Niv Cohen and Yedid Hoshen. Sub-image anomaly detection with deep pyramid correspondences. *ArXiv*, abs/2005.02357, 2020. 1, 2
- [7] Thomas Defard, Aleksandr Setkov, Angélique Loesch, and Romaric Audigier. Padim: a patch distribution modeling framework for anomaly detection and localization. In *ICPR Workshops*, 2020. 2
- [8] Hanqiu Deng and Xingyu Li. Anomaly detection via reverse distillation from one-class embedding. In *Proceedings of the IEEE/CVF Conference on Computer Vision and Pattern Recognition (CVPR)*, pages 9737–9746, 2022. 1, 2
- [9] Choubo Ding, Guansong Pang, and Chunhua Shen. Catching both gray and black swans: Open-set supervised anomaly detection\*. *2022 IEEE/CVF Conference on Computer Vision and Pattern Recognition (CVPR)*, pages 7378–7388, 2022. 2
- [10] Jongheon Jeong, Yang Zou, Taewan Kim, Dongqing Zhang, Avinash Ravichandran, and Onkar Dabeer. Winclip: Zero-/few-shot anomaly classification and segmentation. *2023 IEEE/CVF Conference on Computer Vision and Pattern Recognition (CVPR)*, pages 19606–19616, 2023. 1, 3, 6, 7
- [11] Yunseung Lee and Pilsung Kang. Anovit: Unsupervised anomaly detection and localization with vision transformer-based encoder-decoder. *IEEE Access*, 10:46717–46724, 2022. 1, 2
- [12] Bo Li, Yuanhan Zhang, Liangyu Chen, Jinghao Wang, Jingkang Yang, and Ziwei Liu. Otter: A multi-modal model with in-context instruction tuning. *ArXiv*, abs/2305.03726, 2023. 2
- [13] Chun-Liang Li, Kihyuk Sohn, Jinsung Yoon, and Tomas Pfister. Cutpaste: Self-supervised learning for anomaly detection and localization. *2021 IEEE/CVF Conference on Computer Vision and Pattern Recognition (CVPR)*, pages 9659–9669, 2021. 2
- [14] Yufei Liang, Jiangning Zhang, Shiwei Zhao, Ru-Chwen Wu, Yong Liu, and Shuwen Pan. Omni-frequency channel-selection representations for unsupervised anomaly detection. *IEEE Transactions on Image Processing*, 32:4327–4340, 2022. 2
- [15] Tsung-Yi Lin, Priya Goyal, Ross B. Girshick, Kaiming He, and Piotr Dollár. Focal loss for dense object detection. *2017 IEEE International Conference on Computer Vision (ICCV)*, pages 2999–3007, 2017. 6
- [16] Haotian Liu, Chunyuan Li, Qingyang Wu, and Yong Jae Lee. Visual instruction tuning. *ArXiv*, abs/2304.08485, 2023. 2
- [17] Anqi Mao, Mehryar Mohri, and Yutao Zhong. Cross-entropy loss functions: Theoretical analysis and applications. *ArXiv*, abs/2304.07288, 2023. 6
- [18] Fausto Milletari, Nassir Navab, and Seyed-Ahmad Ahmadi. V-Net: Fully Convolutional Neural Networks for Volumetric Medical Image Segmentation. In *2016 Fourth International Conference on 3D Vision (3DV)*, pages 565–571, Los Alamitos, CA, USA, 2016. IEEE Computer Society. 6
- [19] Alec Radford, JongWook Kim, Chris Hallacy, A. Ramesh, Gabriel Goh, Sandhini Agarwal, Girish Sastry, Askell Amanda, Pamela Mishkin, Jack Clark, Gretchen Krueger, and Ilya Sutskever. Learning transferable visual models from natural language supervision. *Cornell University - arXiv*, *Cornell University - arXiv*, 2021. 1, 2, 3
- [20] Yongming Rao, Wenliang Zhao, Guangyi Chen, Yansong Tang, Zheng Zhu, Guan Huang, Jie Zhou, and Jiwen Lu. Denseclip: Language-guided dense prediction with context-aware prompting. In *2022 IEEE/CVF Conference on Computer Vision and Pattern Recognition (CVPR)*, 2022. 1, 2, 3
- [21] Tal Reiss, Niv Cohen, Liron Bergman, and Yedid Hoshen. Panda: Adapting pretrained features for anomaly detection and segmentation. In *Proceedings of the IEEE/CVF Conference on Computer Vision and Pattern Recognition (CVPR)*, pages 2806–2814, 2021. 1, 2
- [22] Karsten Roth, Latha Pemula, Joaquin Zepeda, Bernhard Scholkopf, Thomas Brox, and Peter Gehler. Towards total recall in industrial anomaly detection. *2022 IEEE/CVF Conference on Computer Vision and Pattern Recognition (CVPR)*, pages 14298–14308, 2021. 2
- [23] Marco Rudolph, Tom Wehrbein, Bodo Rosenhahn, and Bastian Wandt. Fully convolutional cross-scale-flows for image-based defect detection. In *Proceedings of the IEEE/CVF Winter Conference on Applications of Computer Vision (WACV)*, pages 1088–1097, 2022.
- [24] Qian Wan, Yunkang Cao, Liang Gao, Weiming Shen, and Xinyu Li. Position encoding enhanced feature mapping for image anomaly detection. In *2022 IEEE 18th International Conference on Automation Science and Engineering (CASE)*, pages 876–881. IEEE, 2022. 1
- [25] Qian Wan, Liang Gao, Xinyu Li, and Long Wen. Unsupervised image anomaly detection and segmentation based on pretrained feature mapping. *IEEE Transactions on Industrial Informatics*, 19:2330–2339, 2023.

- [26] Guodong Wang, Shumin Han, Errui Ding, and Di Huang. Student-teacher feature pyramid matching for anomaly detection. In *British Machine Vision Conference*, 2021. 1
- [27] Guodong Wang, Shumin Han, Errui Ding, and Di Huang. Student-teacher feature pyramid matching for anomaly detection. In *British Machine Vision Conference*, 2021. 2
- [28] Julian Wyatt, Adam Leach, Sebastian M Schmon, and Chris G Willcocks. Anodpdm: Anomaly detection with denoising diffusion probabilistic models using simplex noise. In *Proceedings of the IEEE/CVF conference on computer vision and pattern recognition*, pages 650–656, 2022. 1, 2
- [29] Xudong Yan, Huaidong Zhang, Xuemiao Xu, Xiaowei Hu, and Pheng-Ann Heng. Learning semantic context from normal samples for unsupervised anomaly detection. In *Proceedings of the AAAI conference on artificial intelligence*, pages 3110–3118, 2021.
- [30] Yi Yan, Deming Wang, Guangliang Zhou, and Qijun Chen. Unsupervised anomaly segmentation via multilevel image reconstruction and adaptive attention-level transition. *IEEE Transactions on Instrumentation and Measurement*, 70:1–12, 2021.
- [31] Jie Yang, Yong Shi, and Zhiquan Qi. Dfr: Deep feature reconstruction for unsupervised anomaly segmentation. *arXiv preprint arXiv:2012.07122*, 2020. 2
- [32] Minghui Yang, Peng Wu, Jing Liu, and Hui Feng. Memseg: A semi-supervised method for image surface defect detection using differences and commonalities. *Eng. Appl. Artif. Intell.*, 119:105835, 2022. 1, 2
- [33] Zhiyuan You, Lei Cui, Yujun Shen, Kai Yang, Xin Lu, Yu Zheng, and Xinyi Le. A unified model for multi-class anomaly detection. *ArXiv*, abs/2206.03687, 2022. 2
- [34] Zhiyuan You, Kai Yang, Wenhan Luo, Lei Cui, Yu Zheng, and Xinyi Le. Adtr: Anomaly detection transformer with feature reconstruction. In *International Conference on Neural Information Processing*, pages 298–310. Springer, 2022. 1, 2
- [35] Jiawei Yu1, Ye Zheng, Xiang Wang, Wei Li, Yushuang Wu, Rui Zhao, and Liwei Wu. Fastflow: Unsupervised anomaly detection and localization via 2d normalizing flows. *ArXiv*, abs/2111.07677, 2021. 1, 2
- [36] Kang Zhou, Yuting Xiao, Jianlong Yang, Jun Cheng, Wen Liu, Weixin Luo, Zaiwang Gu, Jiang Liu, and Shenghua Gao. Encoding structure-texture relation with p-net for anomaly detection in retinal images. *ArXiv*, abs/2008.03632, 2020. 2
- [37] Kaiyang Zhou, Jingkang Yang, Chen Change Loy, and Ziwei Liu. Learning to prompt for vision-language models. *International Journal of Computer Vision*, 130:2337 – 2348, 2021. 1, 2, 3
- [38] Kaiyang Zhou, Jingkang Yang, Chen Change Loy, and Ziwei Liu. Conditional prompt learning for vision-language models. *2022 IEEE/CVF Conference on Computer Vision and Pattern Recognition (CVPR)*, pages 16795–16804, 2022. 1, 2
- [39] Qihang Zhou, Guansong Pang, Yu Tian, Shibo He, and Jiming Chen. Anomalyclip: Object-agnostic prompt learning for zero-shot anomaly detection. *ArXiv*, abs/2310.18961, 2023. 1, 2, 3, 6, 7
- [40] Yang Zou, Jongheon Jeong, Latha Pemula, Dongqing Zhang, and Onkar Dabeer. Spot-the-difference self-supervised pre-training for anomaly detection and segmentation. In *European Conference on Computer Vision*, 2022. 2
- [41] Yang Zou, Jongheon Jeong, Latha Pemula, Dongqing Zhang, and Onkar Dabeer. Spot-the-difference self-supervised pre-training for anomaly detection and segmentation. In *European Conference on Computer Vision*, 2022. 2, 6